Article

Current Biology

# Investigating the Regulation of Stem and Progenitor Cell Mitotic Progression by In Situ Imaging

## Graphical Abstract

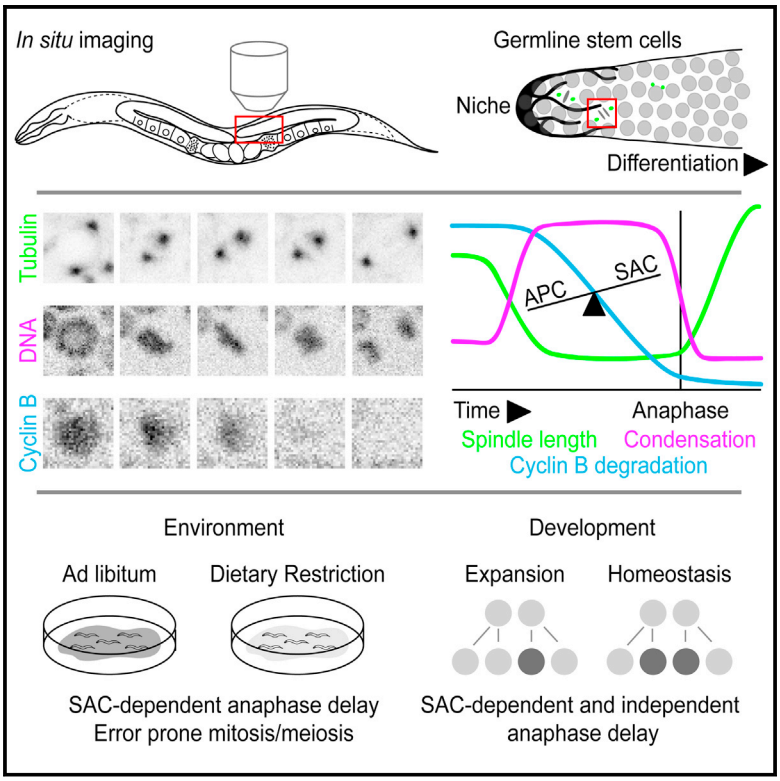


## Highlights

- The SAC regulates mitotic timing *C. elegans* germline stem and progenitor cells
- As in cultured cells, SAC inhibition of the APC is graded rather than absolute
- Dietary restriction causes SAC-dependent delays in germline stem and progenitor cells
- Adult cells show SAC-dependent and -independent changes in mitotic progression

## Authors

Abigail R. Gerhold, Joël Ryan, ..., Jean-Claude Labbé, Paul S. Maddox

## Correspondence

jc.labbe@umontreal.ca (J.-C.L.), pmaddox@unc.edu (P.S.M.)

## In Brief

Gerhold et al. describe the quantitative in situ live imaging of several dynamic processes during *C. elegans* germline stem and progenitor cell mitosis. They find that mitotic checkpoint regulation in germline stem and progenitor cells is similar to that in cultured mammalian cells and that mitotic progression is sensitive to physiological changes.

Gerhold et al., 2015, Current Biology *25*, 1123–1134
May 4, 2015 
http://dx.doi.org/10.1016/j.cub.2015.02.054

CellPress

Current Biology
Article

# Investigating the Regulation of Stem and Progenitor Cell Mitotic Progression by In Situ Imaging

Abigail R. Gerhold,[1] Joël Ryan,[1] Julie-Nathalie Vallée-Trudeau,[1] Jonas F. Dorn,[1] Jean-Claude Labbé,[1,2,*] and Paul S. Maddox[3,*]
[1]Institute of Research in Immunology and Cancer (IRIC)
[2]Department of Pathology and Cell Biology
Université de Montréal, C.P. 6128, Succursale Centre-ville, Montréal, QC H3C 3J7, Canada
[3]Department of Biology, University of North Carolina at Chapel Hill, Chapel Hill, NC 27599, USA
*Correspondence: jc.labbe@umontreal.ca (J.-C.L.), pmaddox@unc.edu (P.S.M.)
http://dx.doi.org/10.1016/j.cub.2015.02.054

## SUMMARY

**Genome stability relies upon efficacious chromosome congression and regulation by the spindle assembly checkpoint (SAC). The study of these fundamental mitotic processes in adult stem and progenitor cells has been limited by the technical challenge of imaging mitosis in these cells in situ. Notably, how broader physiological changes, such as dietary intake or age, affect mitotic progression in stem and/or progenitor cells is largely unknown. Using in situ imaging of *C. elegans* adult germlines, we describe the mitotic parameters of an adult stem and progenitor cell population in an intact animal. We find that SAC regulation in germline stem and progenitor cells is distinct from that found in early embryonic divisions and is more similar to that of classical tissue culture models. We further show that changes in organismal physiology affect mitotic progression in germline stem and progenitor cells. Reducing dietary intake produces a checkpoint-dependent delay in anaphase onset, and inducing dietary restriction when the checkpoint is impaired increases the incidence of segregation errors in mitotic and meiotic cells. Similarly, developmental aging of the germline stem and progenitor cell population correlates with a decline in the rate of several mitotic processes. These results provide the first in vivo validation of models for SAC regulation developed in tissue culture systems and demonstrate that several fundamental features of mitotic progression in adult stem and progenitor cells are highly sensitive to organismal physiological changes.**

## INTRODUCTION

The ability of adult stem and progenitor cells to maintain tissue homeostasis over the lifetime of an organism requires the faithful execution of mitosis under a wide range of physiological conditions. Successful cell division hinges on the fidelity of chromosome segregation, which relies on efficient spindle assembly and the activity of the spindle assembly checkpoint (SAC). During prometaphase, replicated chromosome pairs connect to opposite spindle poles via kinetochore-microtubule attachments and congress to the metaphase plate. The SAC monitors this process and prevents anaphase onset until all kinetochore-microtubule attachments have been made and proper, bi-oriented alignment has been achieved. Failure of the SAC can lead to chromosome segregation errors, aneuploidy, genome instability, and the development of cancer.

While spindle assembly and SAC regulation have been studied extensively in cultured cells and during early embryonic divisions, very little is known about how they occur when cells divide within the complex physiological environment of a mature organism. Notably, despite recent advancements in intravital imaging of certain murine stem cell populations [1–4], fundamental features of mitotic progression have not been carefully characterized in an adult stem or progenitor cell population. Thus, understanding how the highly dynamic events of mitosis are affected by the broader physiological context within which a cell divides constitutes a significant gap in the field of cell biology.

*C. elegans* provides an excellent model system in which to address this challenge. The *C. elegans* adult hermaphrodite gonad houses two pools of undifferentiated, mitotically active germ cells located at the distal end of the two gonad arms (Figure 1A). All other cells in the adult worm are non-proliferative. The zone of mitotic germ cells includes a distal pool of germline stem cells (GSCs) and a more proximal region of proliferative progenitor cells that are more committed to differentiation [5–7]. GSCs undergo self-renewing divisions to maintain stem cell number while also sustaining gamete production and are maintained by proximity-based niche interactions [7–11]. Studies conducted in the *C. elegans* embryo suggest that the SAC is dispensable for early cell divisions and only weakly inducible upon spindle disruption [12, 13]. However, depletion of SAC genes results in post-embryonic defects that are consistent with the SAC playing a more prominent role in the germline [14]. Adult worms are small (~1 mm) and transparent, with the adult gonad and mitotic stem and progenitor cells being readily visible in whole-mounted, intact animals (Figure 1B). Thus, they provide an excellent model system in which to study mitosis and SAC regulation in vivo directly by live imaging.

Live imaging of mitosis in an intact organism provides the unique opportunity to ask how mitotic events are influenced by

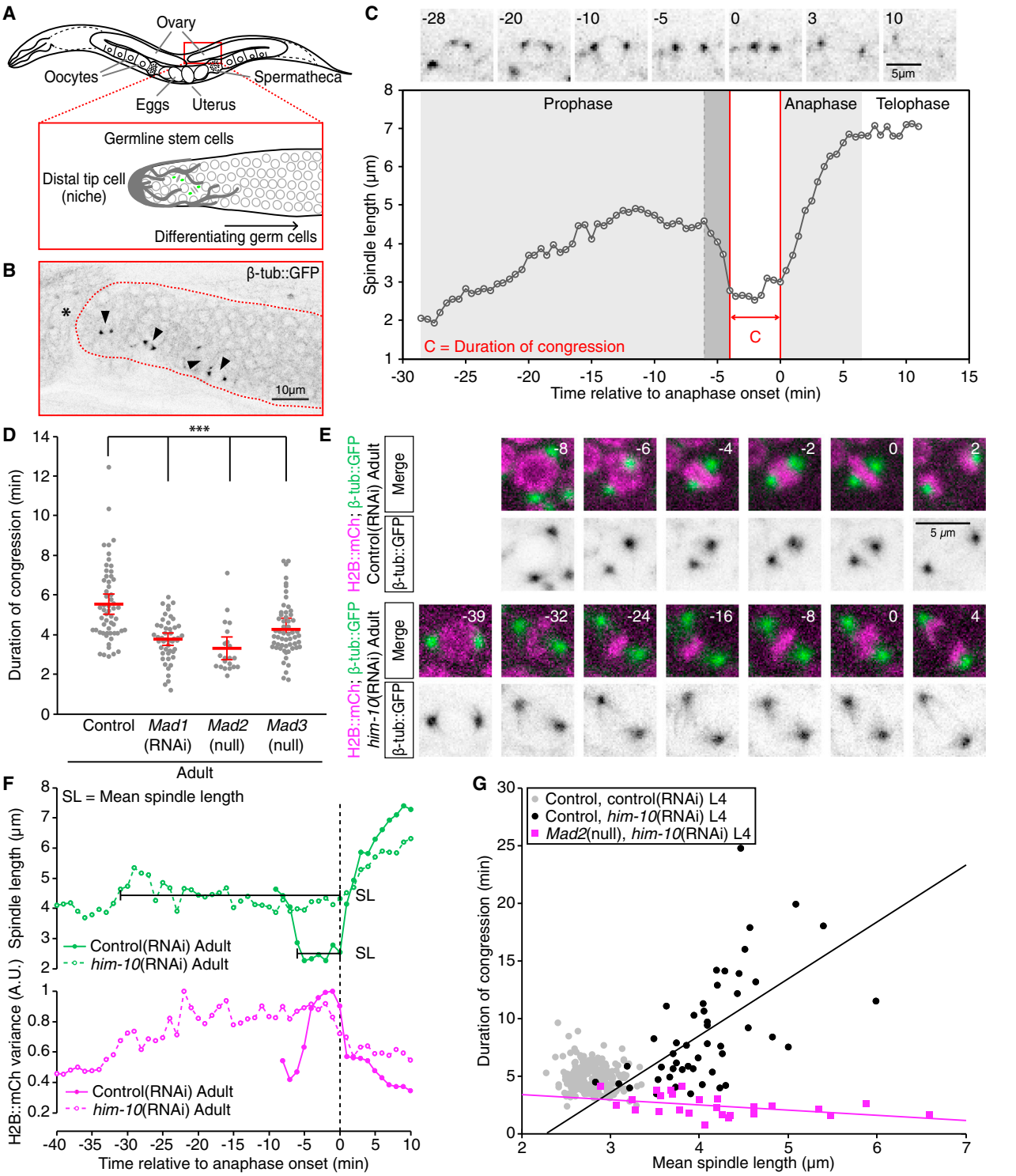


**Figure 1. In Situ Imaging of Spindle Dynamics Reveals SAC Regulation of Mitotic Timing in GSPCs**

(A) Schematic showing the position of germline stem cells within the *C. elegans* gonad.

(B) Maximum-intensity projection of the distal end of an adult gonad in situ, with GSPCs expressing β-tub::GFP. Arrowheads indicate GSPCs in various stages of mitosis. The asterisk (*) marks the distal end of gonad.

(C) Representative graph of spindle length over time for a single GSPC division with the different stages of mitosis indicated. The shaded region at the end of prophase shows the approximate time of nuclear envelope breakdown (NEBD). Single time points from the graphed division are shown above.

*(legend continued on next page)*

**Table 1. Summary of the Features of Adult GSPC Mitosis from Live Imaging of Spindle Dynamics**

| Mitosis | | | | | | |
|---|---|---|---|---|---|---|
| Prophase (min) | Congression/ Metaphase (min) | Anaphase (min) | Spindle Length (μm)[a] | Maximum Spindle Length (μm) | Rate of Spindle Elongation (μm/min)[b] | Pole Separation (μm)[c] |
| 18.9 ± 4 (n = 9) | 5.8 ± 1.7 (n = 99) | 7.2 ± 1.6 (n = 25) | 2.8 ± 0.3 (n = 99) | 7.2 ± 0.7 (n = 25) | 1.3 ± 0.4 (n = 96) | 2.7 ± 0.7 (n = 92) |

Data are presented as mean ± SD. n, number of cells for which a given measurement was made. See also Table S2.
[a]Mean spindle length during congression/metaphase.
[b]Rate of spindle elongation during rapid phase of elongation.
[c]The amount of spindle elongation, normalized to metaphase spindle length, 2.5 min after anaphase onset.

developmental and physiological changes. Poor nutrient availability can block or reduce stem cell proliferation in a wide range of organisms, including *C. elegans* GSCs and their precursors [15, 16]. However, how limiting dietary intake influences mitotic progression in cells that continue to cycle despite sub-optimal conditions is unknown. In addition, *C. elegans* germline stem and progenitor cells, similar to other stem cell populations, experience developmentally regulated changes in proliferation. During larval development, the number of stem and progenitor cells increases (expansion) to a pool size of 200–250 cells, which are then maintained during adulthood (homeostasis) [7, 10, 17]. Whether mitotic progression is affected by this switch has not been addressed.

Here we report the live imaging of germline stem and progenitor cell mitosis in intact animals. We show that checkpoint regulation in these cells is different than that in early embryonic divisions and that it bears striking similarities to what has been described in cultured cells. Our results indicate that mitotic progression in germline stem and progenitor cells is sensitive to both developmental and dietary changes. We show that germline stem and progenitor cells take longer to satisfy the SAC after dietary restriction and that several phenotypes associated with chromosome segregation errors are enhanced by induction of dietary restriction when the checkpoint is impaired. In addition, we find that spindle assembly and the execution of anaphase entry are slower in adult germline stem and progenitor cells as compared to larval cells engaged in expansion of the stem cell pool.

## RESULTS

### Live Imaging of Spindle Dynamics to Monitor Mitotic Progression In Situ

To visualize the mitotic spindle in germline stem and progenitor cells, we used a *C. elegans* strain that expresses β-tubulin fused to GFP (β-tub::GFP) under the control of a germline-specific promoter. This allowed us to track centrosome pairs and to monitor mitotic progression by measuring spindle length (Figure 1C and Movie S1). Duplicated centrosomes were first detected as adjacent foci, which then separated and migrated to opposite sides of the nucleus. After NEBD, as assessed by the appearance of microtubules in the nuclear space (data not shown), spindle length decreased and remained fairly constant until the onset of pole separation in anaphase. Spindle elongation was biphasic, with spindle length increasing rapidly at first, then slowing, before reaching a stable maximum.

In the *C. elegans* embryo, the majority of chromosome separation is due to spindle pole separation or anaphase B, with anaphase A (chromosome to spindle pole movement) playing a minimal role [18]. We therefore hypothesized that the start of pole separation could serve as a proxy for anaphase onset. To confirm that changes in spindle length were an accurate reflection of mitotic progression in germline stem and progenitor cells, we imaged divisions in a strain co-expressing β-tub::GFP and histone H2B fused to mCherry (H2B::mCh) (Figures 1E and S1A and Movie S2). We found that the start of detectable chromosome condensation and the initiation of chromosome segregation, as assessed by changes in the variance of the H2B::mCh signal, occurred concomitantly with the decrease in spindle length after NEBD and the start of pole separation, respectively (Figures 1F and S1B). Thus, spindle length provides an accurate and facile measurement of mitotic progression in germline stem and progenitor cells.

Using spindle length, we defined several features of germline stem and progenitor cell mitosis (Table 1). To characterize the timing of spindle assembly, chromosome alignment to the metaphase plate and the duration of metaphase, hereafter referred to as the "duration of congression," we measured the time from when spindle length reached a constant minimum after NEBD to the initiation of pole separation (Figure 1C). Notably, we observed that the duration of congression in adult germline

(D) The distribution of congression timing measured by spindle length for adult GSPCs during unperturbed mitoses with and without the checkpoint. Error bars indicate the 95% confidence interval for the mean. Data were compared by an ANOVA1 with Tukey-Kramer post hoc test. Control, n = 57; *Mad1*(RNAi), n = 50; *Mad2*(null), n = 21; *Mad3*(null), n = 57. ***p < 0.001.
(E) Single time points from control and HIM-10-depleted adult GSPCs expressing β-tub::GFP and H2B::mCh for the divisions analyzed in (F).
(F) Spindle length and H2B::mCh variance over time for the cells shown in (E) showing the effect of HIM-10 depletion on spindle length during congression. SL, mean spindle length.
(G) Scatter plot showing the relationship between the duration of congression (measured by spindle length) and mean spindle length during congression for GSPCs after HIM-10 depletion, with and without the checkpoint. Data for fourth-larval-stage (L4) GSPCs are shown. Wild-type adult GSPCs showed a similar phenotype after HIM-10 depletion (see E and F; data not shown). Analysis of adult *Mad2* mutants after HIM-10 depletion was complicated by the accumulation of segregation errors. Control, Control(RNAi), n = 240; control, *him-10*(RNAi), n = 50; *Mad2*(null) *him-10*(RNAi), n = 27.
See also Figures S1–S3 and Movies S1 and S2.

stem and progenitor cells is highly variable and, on average, twice as long as in *C. elegans* early blastomeres (germline stem and progenitor cells 5.8 ± 1.7 min versus embryo 2.7 ± 0.6 min [12, 19–22]). We did not observe any differences in the features of mitotic progression between cells adjacent to the niche (stem cells) versus those at more proximal positions (committed mitotic progenitor cells; data not shown). All further analyses considered the pool of mitotic germ cells as a whole, which we will refer to as germline stem and progenitor cells (GSPCs). These results provide the first in vivo measurement of mitotic progression in an intact adult organism and suggest that significant differences exist between early embryonic and adult stem or progenitor cell divisions.

## The SAC Regulates Mitotic Progression in GSPCs

A highly variable duration of congression is a hallmark of an active SAC. The core SAC consists of Mad2, BubR1/Mad3, and Bub3, which bind to the anaphase-promoting complex (APC) co-factor Cdc20 to form the mitotic checkpoint complex, and Bub1, Mad1, and Mps1, which promote mitotic checkpoint complex assembly. By binding Cdc20, the mitotic checkpoint complex prevents the APC from degrading securin and cyclin B, thus blocking chromosome segregation and mitotic exit [23]. All core SAC components are conserved in *C. elegans* except Mps1. For the sake of clarity, we have referred to *C. elegans* SAC factors by their ortholog names (see Table S1).

To test whether the SAC regulates the duration of congression in normally dividing GSPCs, we used spindle length to measure congression in the absence of checkpoint activity using RNAi depletion of MAD1 and putative null alleles of *Mad2* and *Mad3*. Similar to what has been reported for mammalian cultured cells [24, 25], the duration of congression was significantly reduced in all three cases (Figure 1D). Thus, unlike in the early embryo, where removing core checkpoint components does not affect the duration of congression [12, 13], basal mitotic timing in GSPCs is sensitive to loss of the SAC.

To assess whether SAC regulation is more robust in GSPCs than in the early embryo, we perturbed spindle assembly by depleting HIM-10. A member of the NDC80 complex, HIM-10 is required to stabilize kinetochore-microtubule interactions, and depletion of its ortholog Nuf2 from mammalian cell lines results in a SAC-dependent mitotic arrest [19, 26, 27]. Similar to what has been reported for the early C. *elegans* embryo and in mammalian cultured cells [19, 26, 27], depletion of HIM-10 in GSPCs resulted in premature spindle pole separation and an increase in mean spindle length during congression (Figures 1E and 1F; 4.1 ± 0.6 μm *him-10*(RNAi) versus 2.8 ± 0.2 μm Control(RNAi)). This allowed us to use mean spindle length during congression as an indication of the severity of the *him-10*(RNAi) phenotype, which was somewhat variable. Nonetheless, the majority of cells with aberrant spindles had significant delays in mitotic progression (1.5- to 5-fold), which were fully suppressed by loss of *Mad2* (Figure 1G). Thus, in GSPCs, disruption of kinetochore-microtubule attachment leads to a checkpoint-dependent delay in mitotic progression.

Unlike more severe spindle perturbations [28, 29], HIM-10 depletion did not significantly increase the number of mitotically active, phospho-Histone H3-positive nuclei in the germline, although aberrantly large nuclei, presumably resulting from failed mitoses, were occasionally observed (Figure S2). Our measurements are therefore unlikely to capture the maximum mitotic delay possible in GSPCs. Despite this, we note that HIM-10 depletion produced a more robust delay in anaphase onset in GSPCs (4 min or 1.8-fold, on average) than what has been described for the early embryo (34 s or 1.2-fold, on average [19]), suggesting that checkpoint regulation is more stringent in GSPCs.

Canonical SAC signaling involves recruitment of core checkpoint components to unattached kinetochores, and their removal from properly oriented chromosomes is a prerequisite for entry into anaphase [23]. To determine whether SAC components showed a similar pattern of localization in GSPCs, we used live imaging to monitor GFP-tagged Bub3 [13]. Bub3::GFP showed robust enrichment on chromosomes during congression, resolving as paired lines flanking the metaphase plate, and was rapidly depleted upon anaphase onset (Figure S3).

Altogether, these results provide direct evidence that in GSPCs the SAC delays anaphase entry in response to abnormal kinetochore-microtubule attachments. Importantly, regulation of mitotic progression in GSPCs is distinct from that in early embryonic divisions, with GSPCs experiencing significantly longer, SAC-regulated durations of congression even in the absence of spindle perturbations. In this regard, checkpoint activity in GSPCs more closely resembles what has been observed in tissue culture studies.

## SAC Inhibition of APC Activity in GSPCs Is Graded Rather Than Absolute

Recent work in cultured mammalian cells has demonstrated that the SAC, rather than acting as an absolute inhibitor, impedes APC activity in proportion to the strength of a given spindle assembly defect [30, 31]. To test whether a similar model held true for checkpoint regulation in GSPCs, we measured APC activity by monitoring the degradation of a cyclin B1-YFP fusion protein (CYB-1::YFP; Figure 2A and Movie S3), as has been used to monitor APC activity in mammalian cell lines [30, 32]. We used the variance of the H2B::mCh signal to monitor mitotic progression (as described above) and plotted bleach-corrected, normalized CYB-1::YFP fluorescence intensity as a function of time relative to anaphase onset. We then fit a sigmoidal function to the CYB-1::YFP degradation curve, which allowed us to compare the degradation parameters between cells (Figure 2B). Partial depletion of CDC20 (FZY-1) and the APC subunit APC-6 (EMB-27) decreased the rate of CYB-1::YFP degradation, indicating that our assay could reliably detect changes in APC activity (Figure S4).

The average CYB-1::YFP degradation curves for GSPCs, with and without checkpoint activity, revealed substantial differences in the kinetics of CYB-1::YFP proteolysis. Elimination of the SAC increased the rate of CYB-1::YFP degradation (Figures 2C and 2E), indicating that during unperturbed divisions the SAC restrains APC activity. Disrupting spindle formation by depleting HIM-10, rather than delaying the onset of CYB-1::YFP degradation, substantially slowed the rate at which CYB-1::YFP was degraded (note the absence of a delay between the start of CYB-1::YFP degradation and the start of congression; Figures 2D and 2F). Overall, the rate of CYB-1::YFP degradation correlated strongly with the duration of mitosis ($r = 0.89$; Figure 2G).

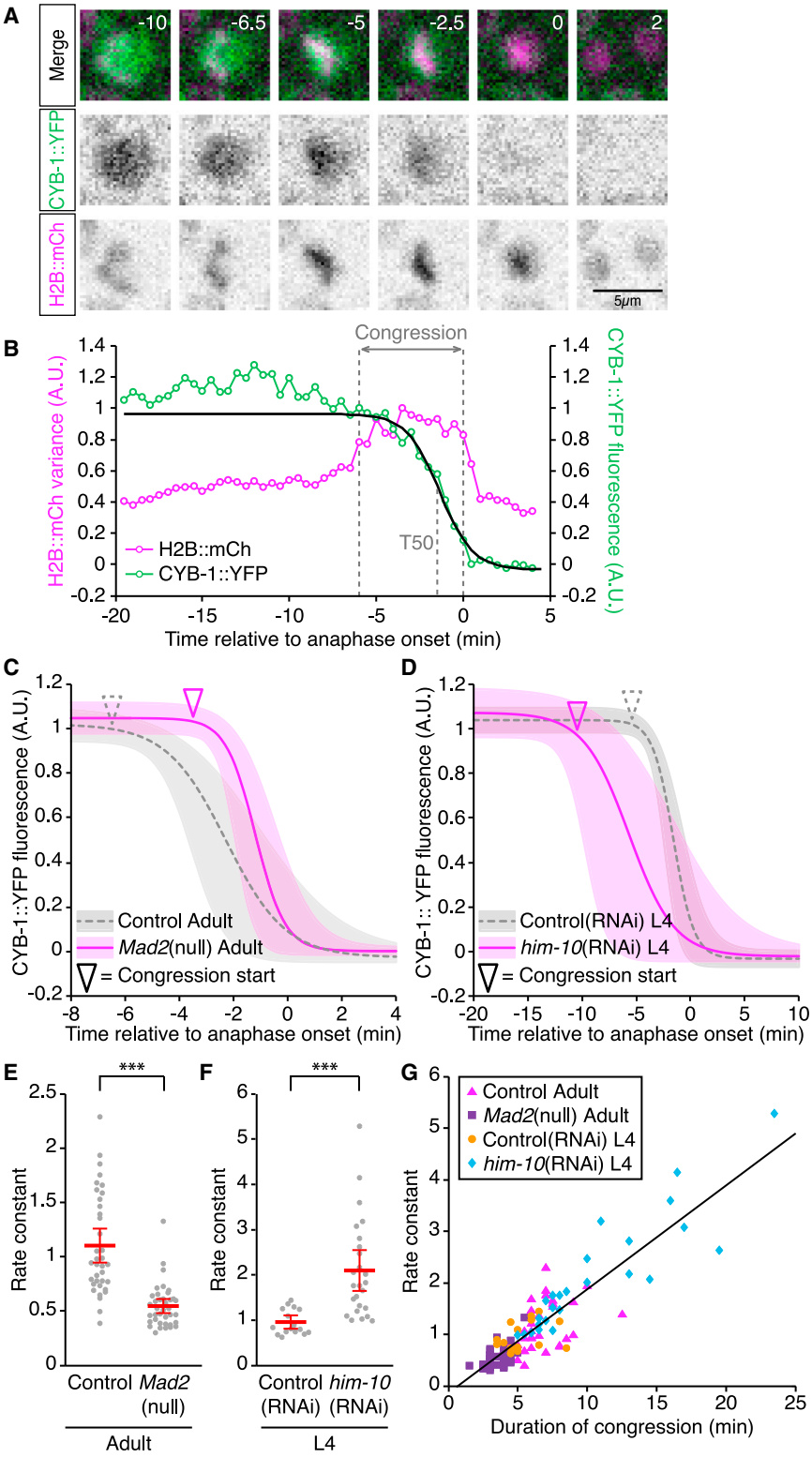


**Figure 2. The SAC Inhibits the APC in a Graded, Rather Than Absolute Manner**

(A) Single time points from an adult GSPC expressing H2B::mCh and CYB-1::YFP showing the division graphed in (B).

(B) Measurements of H2B::mCh variance and CYB-1::YFP fluorescence over time for the division shown in (A). The CYB-1::YFP fluorescence values predicted by the best-fit sigmoid curve are shown in black. T50, time to half maximum.

(C and D) The mean best-fit sigmoid curves (lines) ±1 SD (shaded regions) for CYB-1::YFP degradation, derived from all cells analyzed for each condition. Degradation curves are shown relative to the time of anaphase onset. Triangles indicate the average start of congression for each genotype or condition. (C) Control versus *Mad2*(-null) adult GSPCs. (D) Fourth-larval-stage (L4) GSPCs from animals fed control versus *him-10* RNAi.

(E) The distribution of rate constants for CYB-1::YFP degradation from control and *Mad2*(null) GSPCs.

(F) The distribution of rate constants for CYB-1::YFP degradation from L4 animals after HIM-10 depletion versus controls.

(G) Scatter plot showing the correlation between the rate constant for CYB-1::YFP degradation and the duration of congression (measured by H2B::mCh variance) for all cells analyzed. Pearson's coefficient r = 0.89, Student's t test $p < 0.001$.

For (E) and (F), error bars show the 95% confidence interval for the mean, and data were compared using a Student's t test (***$p < 0.001$). For (C) and (E), control, n = 36; *Mad2*(null), n = 38. For (D) and (F), Control(RNAi), n = 16; *him-10*(RNAi), n = 25. See also Figure S4 and Movie S3.

Given these observations, we conclude that in GSPCs, similarly to mammalian cultured cells, the SAC limits, rather than absolutely inhibits, the APC and that the strength of the SAC scales with the strength of kinetochore-microtubule attachment defects.

## Dietary Restriction Delays Mitotic Progression in GSPCs and Enhances the Requirement for SAC Regulation to Prevent Segregation Errors

Having established the basic parameters of SAC activity in GSPCs, we next asked how mitosis was affected by nutrient availability. We assessed the impact of dietary restriction on mitosis in GSPCs by using spindle length to measure the duration of congression in animals bearing a mutation in *eat-2* (*eat-2(ad465)*, hereafter *eat*-2), which reduces pharyngeal pumping and therefore food intake, and in animals fed a restricted concentration of bacteria ("sDR"; [33, 34]). Both treatments strongly delayed mitotic progression in GSPCs (Figures 3A and 3B).

Dietary restriction affects metabolism and can reduce organismal energy levels [33, 35]. Spindle assembly is highly energy dependent, requiring the activity of force-generating molecular

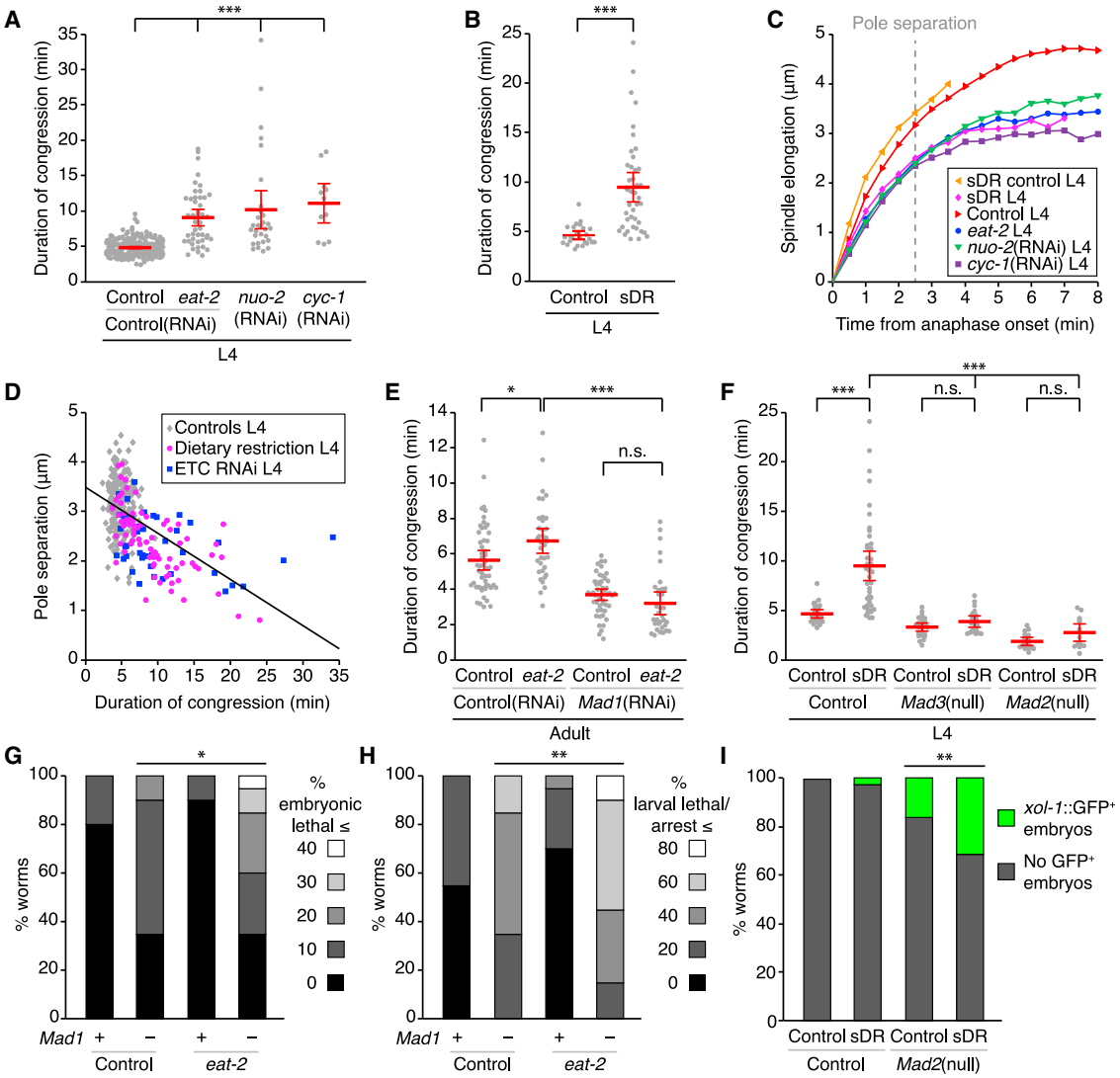


**Figure 3. Dietary Restriction Delays Mitotic Progression and Increases the Incidence of Segregation Errors when the Checkpoint Is Impaired**

(A) The distribution of congression timing measured by spindle length for GSPCs from fourth-larval-stage (L4) *eat-2* mutants and from animals after RNAi depletion of NUO-2 and CYC-1. Control data are reproduced from Figure 1G. Data were compared using an ANOVA1 with Tukey-Kramer post hoc test. *eat-2*, n = 46; *nuo-2*(RNAi), n = 30; *cyc-1*(RNAi), n = 12.

(B) The distribution of congression timing measured by spindle length for GSPCs from L4 animals subjected to sDR versus controls. Data were compared using a Student's t test. Control, n = 25; sDR, n = 42.

(C) Mean spindle elongation (spindle length during anaphase relative to metaphase) over time for the cells analyzed in (A) and (B). Dashed line marks the time (2.5 min after anaphase onset) at which pole separation values were extracted.

(D) Scatter plot showing the relationship between the amount of spindle elongation achieved at 2.5 min after anaphase onset (pole separation) versus the duration of congression for single GSPCs. ETC (electron transport chain) denotes data from NUO-2 and CYC-1 depletions. $r = -0.55$, $p < 0.001$. p values for Pearson's coefficient (r) were determined by a Student's t test.

(E and F) The distribution of congression timing measured by spindle length upon dietary restriction with and without the checkpoint. Data were compared using an ANOVA1 with Tukey-Kramer post hoc test. (E) *eat-2* mutant adult animals ± *Mad1*(RNAi). Control data are reproduced from Figure 1D. *eat-2* Control(RNAi), n = 36; *eat-2 Mad1*(RNAi), n = 32. (F) Control L4 animals subjected to sDR compared to *Mad2* and *Mad3* mutants. Control ± sDR data are reproduced from (B). *Mad3*(null) control, n = 24; *Mad3*(null) sDR, n = 19; *Mad2*(null) control, n = 17; *Mad2*(null) sDR, n = 14.

(G and H) The effect of MAD1 depletion in control versus *eat-2* mutant animals on embryonic lethality (G) and larval lethality and/or arrest (H). Data were binned according to the intervals shown at the right of each graph (e.g., in G, white represents the percentage of worms with 30% < embryonic lethality ≤ 40%). Data were compared by a two-tailed Student's t test.

(I) The effect of sDR on the percentage of animals with $GFP^+$ embryos in wild-type versus *Mad2* mutant animals. GFP is expressed only in male embryos, which are the result of X chromosome segregation errors. Data were compared by a two-sided Wilcoxon rank-sum test.

For (A), (B), (E), and (F), error bars show the 95% confidence interval for the mean. For all panels, ***$p < 0.001$, **$p < 0.01$, and *$p < 0.05$; n.s. (not significant), $p > 0.05$.

**Table 2. The Number of Mitotic Cells per Gonad Arm and the Approximate Mitotic Index in GSPCs during Expansion and Homeostasis of the Stem Cell Pool**

| | Expansion | | | | Homeostasis | |
|---|---|---|---|---|---|---|
| | Early L4 | Mid L4 | Late L4 | YA | 1-Day-Old Adult | 2-Day-Old Adult |
| Mitotic cells per gonad arm[a] | 10.3 ± 2.1 (n = 11) | 13.6 ± 2.8 (n = 8) | 14 ± 4.3 (n = 13) | 15.3 ± 3.5 (n = 3) | 9.7 ± 3.5 (n = 17) | 9.4 ± 3.0 (n = 8) |
| Approximate number of cells per mitotic zone[b] | 90 | 135 | 200 | 200 | 230 | 219 |
| Mitotic index (%) | 11.4 ± 2.1 | 10.1 ± 2.1 | 7 ± 2.1 | 7.6 ± 1.8 | 4.2 ± 1.5 | 4.3 ± 1.4 |

Data are presented as mean ± SD. n, number of gonad arms analyzed.
[a]Number of cells with two defined centrosomes at the first time frame of each time-lapse acquisition.
[b]Values were derived from two published reports of the number of cells in the mitotic zone at different developmental stages [17, 34].

motors and other ATP- and GTPases, including tubulin [36]. Thus, dietary restriction may prolong the duration of congression by limiting the amount of energy available to GSPCs. If so, other energy-dependent mitotic processes, such as spindle elongation during anaphase [37], should be similarly affected. Indeed, the rate of spindle elongation was reduced after dietary restriction, and the duration of congression correlated with the rate of spindle elongation ($r = -0.55$; Figures 3C and 3D). To directly test whether reduction of energy (ATP) at the organismal level affected congression in GSPCs, we depleted two components of the electron transport chain (NUO-2 and CYC-1; [38]). Depletion of either NUO-2 or CYC-1 strongly extended the duration of congression and slowed the rate of spindle elongation in anaphase (Figures 3A and 3C and 3D), suggesting that dividing GSPCs are highly sensitive to organismal energy levels.

We next tested whether the increased duration of congression after dietary restriction required SAC regulation. Indeed, the delay in mitotic progression produced by both *eat-2* mutation and sDR was largely dependent on a functional checkpoint (Figures 3E and 3F). Taken together, our results are consistent with a model in which energy-dependent mitotic processes, such as spindle assembly, are slower in GSPCs subjected to dietary restriction, thereby increasing the amount of time required for these cells to satisfy the SAC.

If dietary restriction slows spindle assembly, we would expect that it might also increase the likelihood of segregation errors in the absence of SAC regulation. To test this hypothesis, we determined whether removing the SAC in combination with dietary restriction enhanced phenotypes related to chromosome segregation errors. Depletion of MAD1 in *C. elegans* leads to an increase in embryonic lethality and larval lethality or arrest due to the accumulation of segregation errors in both germ and somatic cells [28]. We found that depleting MAD1 by RNAi in an *eat-2* mutant background increased the severity of both of these phenotypes (Figures 3G and 3H). We next used a GFP reporter (*xol-1::GFP*) that is expressed specifically in XO embryos, which, in non-mated hermaphrodites (XX), are due predominantly to meiotic X chromosome segregation errors [39, 40]. We found that more *Mad2* mutant animals produced GFP-positive embryos than did wild-type animals and that this phenotype was enhanced by subjecting worms to sDR (Figure 3I). While these results do not distinguish between errors incurred in GSPCs versus those occurring in somatic cells and during oogenesis, they are consistent with a general, enhanced requirement for SAC surveillance to prevent chromosome segregation errors after dietary restriction.

## Mitotic Timing Is Affected by the Developmental Transition between Expansion and Homeostasis

We next asked whether the rate of mitotic progression is affected by the developmentally regulated switch from expansion to homeostasis of the GSPC pool. After the transition to homeostasis, we observed a decrease in the number of mitotic cells per a gonad arm, which, given the greater absolute number of GSPCs and the observation that no quiescent cells exist within the adult GSPC pool [7, 8, 17, 34], suggests an overall slowing of the cell cycle (Table 2). To determine whether mitotic progression was also affected by this transition, we used spindle length to measure the duration of congression at four time points during expansion (early-, mid-, and late-fourth larval stage [L4] and young adults [YAs]) and at two time points during homeostasis (1- and 2-day-old adults). While the average duration and the variance of congression remained fairly constant throughout expansion, both factors increased after the transition to homeostasis (Figure 4A and Table S2).

Several metabolic indices, including organismal ATP levels, are reduced in mature adult animals as compared to developing larvae [41]. Thus, we tested whether in adult GSPCs, as in cells subjected to dietary restriction, other energy-dependent mitotic processes were also affected. Indeed, the rate of anaphase spindle elongation was reduced (Figures 4B and 4C), suggesting that decreased energy availability contributes to longer durations of congression in adult GSPCs. However, unlike in GSPCs subjected to dietary restriction, the increased duration of congression in adult cells was partially checkpoint independent. In the absence of checkpoint regulation, adult GSPCs still took longer to enter anaphase than did larval cells (Figure 4D), suggesting that energy-related delays in spindle assembly are not the sole determinant of slower mitotic progression in adult cells.

In the absence of the SAC, anaphase onset is determined by the amount of time required for the proteolysis of securin and cyclin B by the APC [42, 43]. To test whether the SAC-independent mitotic delay that we observed in adult GSPCs was due to lower levels of APC activity, we measured CYB-1::YFP degradation to assess APC activity in larval versus adult cells. While the rate of CYB-1::YFP degradation was significantly slower in adult cells, removing the checkpoint largely eliminated this difference (Figures 4E–4G). Thus, slower CYB-1::YFP degradation in adult cells largely reflects increased SAC activity. We note, however, that

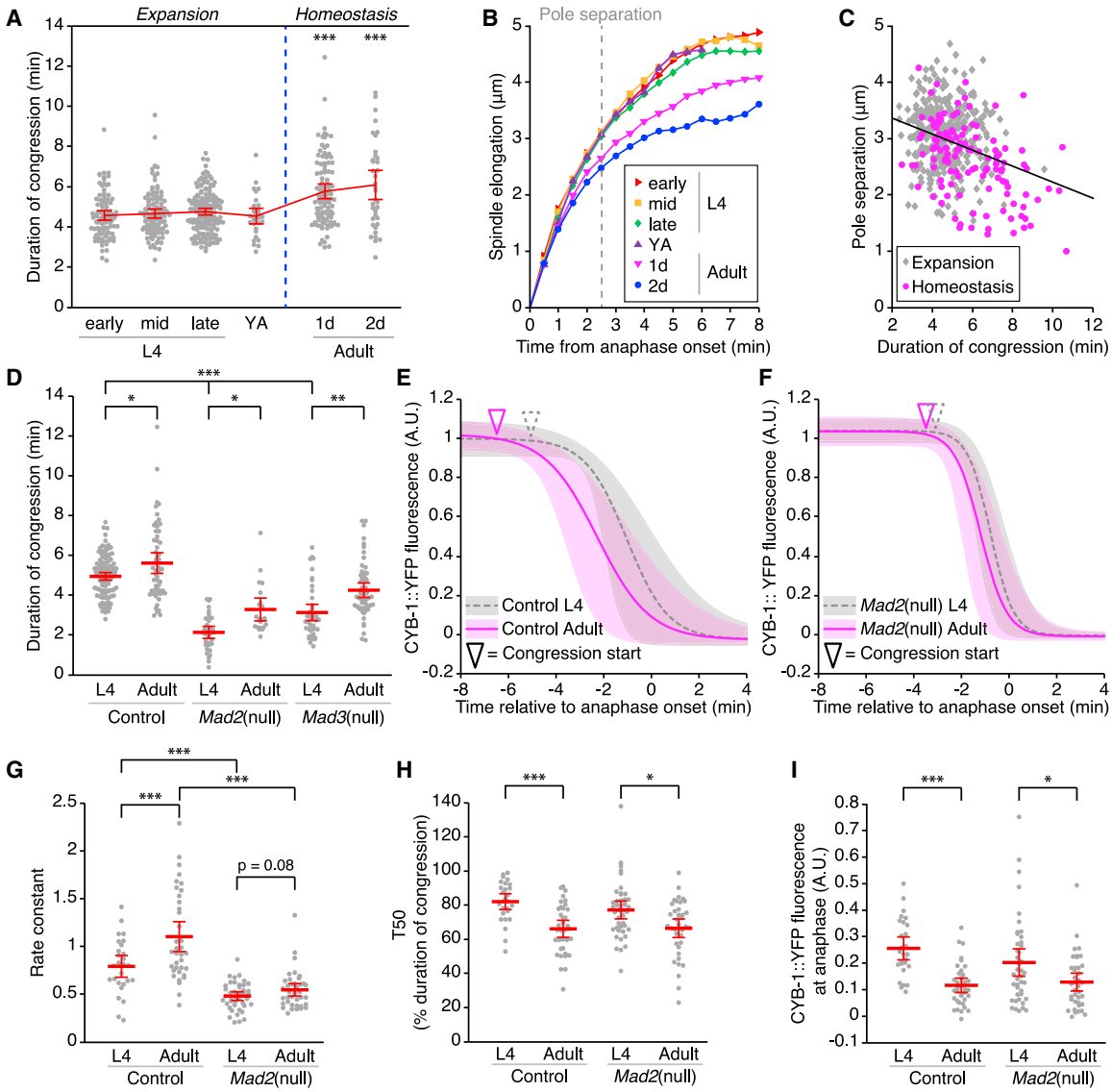


**Figure 4. Adult GSPCs Exhibit SAC-Dependent and -Independent Delays in Mitotic Progression Relative to Cells Participating in Expansion of the Stem Cell Pool**

(A) The duration of congression measured by spindle length for GSPCs analyzed at the developmental stages specified. L4, fourth larval stage; YA, young adult. Data for 1- and 2-day-old adults were significantly different (***$p < 0.001$) from all expansion time points. No other comparisons yielded significant differences. Early L4, n = 92; mid L4, n = 104; late L4, n = 156; YA, n = 30; 1-day-old adult, n = 99; 2-day-old adult, n = 37.

(B) Mean spindle elongation (spindle length during anaphase relative to metaphase) over time for GSPCs analyzed in (A). Dashed line marks the time (2.5 min after anaphase onset) at which pole separation values were extracted.

(C) Scatter plot showing the relationship between the amount of spindle elongation achieved at 2.5 min after anaphase onset (pole separation) versus the duration of congression during expansion versus homeostasis for the GSPCs analyzed in (A). $r = -0.33$, $p < 0.001$. p values for Pearson's coefficient (r) were determined by a Student's t test.

(D) The distribution of congression timing measured by spindle length in GSPCs from 1-day-old adults compared to late-L4 animals in control and *Mad2* and *Mad3* mutant backgrounds. Adult data are reproduced from Figure 1D. L4 control, n = 114; L4 *Mad2*(null), n = 35; L4 *Mad3*(null), n = 41.

(E and F) The mean best-fit sigmoid curves (line) ±1 SD (shaded region) for CYB-1::YFP degradation, derived from all cells analyzed for each condition. Degradation curves are shown relative to the time of anaphase onset. Triangles indicate the average start of congression (measured by H2B::mCh variance) for each genotype or condition. (E) Control L4 versus adult GSPCs. (F) *Mad2*(null) L4 versus adult GSPCs. Adult data for (E) and (F) are reproduced from Figure 2C.

(G) The distribution of rate constants for CYB-1::YFP degradation from control and *Mad2*(null) L4 and adult GSPCs. Adult data are reproduced from Figure 2E.

(H) The distribution of time to half maximum (T50) values expressed relative to the timing of congression for GSPCs from control and *Mad2*(null) L4 and adult animals.

(I) The best-fit sigmoid curve for each cell was used to predict the amount of CYB-1::YFP fluorescence remaining at anaphase onset for control and *Mad2*(null) GSPCs from L4 and adult animals.

For (A), (D), and (G)–(I), error bars indicate the 95% confidence interval for the mean and data were compared by an ANOVA1 with Tukey-Kramer post hoc test. For (E)–(I), control L4, n = 27; Mad2(null), L4 n = 42. For all panels, ***$p < 0.001$, **$p < 0.01$, and *$p < 0.05$. See also Table S2.

CYB-1::YFP degradation tended to be more rapid during expansion in *Mad2* mutants ($p = 0.08$), suggesting that subtle differences in APC activity exist between larval and adult GSPCs, independent of checkpoint inhibition.

In comparing CYB-1::YFP degradation curves, we noticed that the time to half maximum (T50) relative to the timing of anaphase onset was significantly different between larval and adult GSPCs. When normalized to the duration of congression, larval cells reached T50 when congression was on average 82% complete, whereas adult cells reached T50 when congression was only 66% complete, a difference that was maintained in *Mad2* mutants (Figure 4I). This shift in T50 toward anaphase onset meant that larval cells entered anaphase with higher levels of CYB-1::YFP than did adult cells (on average, 26% [larval] versus 12% [adult] CYB-1::YFP remaining; Figure 4J). Assuming that the degradation of endogenous APC targets mirrors that of CYB-1::YFP, these results suggest that larval GSPCs also enter anaphase at a higher concentration of cyclin B and securin.

We conclude that adult GSPCs, which exhibit a slower cell cycle, take longer to satisfy the SAC and may have slightly less APC activity. GSPCs undergoing expansion, which are primed to divide more rapidly, exhibit more rapid M phases and may initiate anaphase in the presence of higher levels of APC targets.

## DISCUSSION

Our results provide the first direct measurement of mitotic timing in *C. elegans* GSPCs and are consistent with the checkpoint playing a more prominent role in these cells compared to dividing embryonic blastomeres. We have shown that during normal, unperturbed mitoses, GSPCs take longer to enter anaphase than do early embryonic cells and that elimination of the SAC accelerates mitotic progression substantially. In addition, comparable spindle disruptions generate a more robust delay in anaphase onset in GSPCs than in the early embryo. In these regards, the regulation of mitotic progression in GSPCs more closely resembles that which has been described for mammalian tissue culture cells than for embryonic divisions.

It is becoming increasingly clear that many steps in mitosis are governed by a balance between the competing activities of positive and negative regulators of each transition. In particular, it has been shown recently that the ability of the SAC to block the APC scales with the severity of the induced spindle defect [30, 31]. We have shown that a similar scaling occurs in normally dividing GSPCs, in which the rate rather than the onset of cyclin B degradation is proportional to the duration of congression.

The ability to observe mitosis in intact animals provides the unique opportunity to assess how mitotic progression is influenced by physiological changes. To this end, we have determined that both developmental stage and dietary intake impact the duration of congression in GSPCs. Dietary restriction leads to a checkpoint-dependent delay in anaphase onset. As a second, energy-dependent mitotic process (spindle elongation) is also slowed by dietary restriction, we believe that cells subjected to dietary restriction take longer to satisfy the SAC largely because lower energy levels slow spindle assembly. However, we do not rule out the possibility that more direct regulation also plays a role, potentially via a reduction in the abundance of proteins required for kinetochore and spindle assembly or by an enhancement of checkpoint regulation itself.

Dietary restriction has long been studied for its ability to enhance longevity, delay age-associated deterioration and disease and increase tolerance to acute stressors [44]. Our results suggest that, in addition to these beneficial effects, dietary restriction may negatively impact proliferative tissues by limiting the energy available for and thus slowing mitotic processes, such as spindle assembly. In the absence of checkpoint surveillance, slower spindle assembly increases the likelihood that anaphase entry will occur before proper chromosome alignment is achieved, rendering both mitotic and meiotic cells more error prone. Thus, an evolutionary pressure driving maintenance of the SAC could be the need to buffer mitotically active cells against changing environmental conditions such as food availability. In addition, as cancer cells often exist within nutrient-limited environments [45], our results suggest that the energetic constraints imposed on these dividing cells could be a contributing factor in the development of aneuploidy.

Similarly to dietary restriction, we have found that the duration of congression is increased in adult GSPCs as compared to cells undergoing developmental expansion of the stem and progenitor cell pool. This difference cannot be attributed solely to differences spindle assembly, as it is, in part, checkpoint independent. Instead, adult GSPCs may have slightly lower levels of APC activity. Our data also suggest the possibility that during expansion, GSPCs initiate anaphase entry at a higher concentration of APC substrates. Chromosome separation in anaphase requires the activity of separase, which is inhibited by the APC target securin. Similarly, spindle elongation requires the activation of phosphatases to undo cyclin B-CDK1 phosphorylations. Thus, one hypothesis to explain our results is that the initiation of anaphase in GSPCs, after satisfaction of the SAC, is governed by a balance between the proteolysis of securin and cyclin B and the activity of the enzymes that they counteract. This balance is seemingly tipped to favor anaphase initiation during developmental expansion of the GSPC pool when cells are primed to undergo more frequent divisions.

Overall, we have shown that adult GSPCs have slower mitoses, with congression, anaphase initiation, and spindle elongation all occurring more slowly. These changes occur concomitantly with a decline in the mitotic index. Age-related declines in the regenerative potential of adult tissues have been attributed to a decline in the proliferation of stem or progenitor cells [46]. Our results suggest that the progression through mitosis in those cells that do divide may be compromised even from an early age. Future experiments will determine whether the speed of mitosis continues to decline as adult GSPCs age and, importantly, whether an earlier, more rapid mitotic state can be restored.

## EXPERIMENTAL PROCEDURES

### *C. elegans* Strains and Culture

All strains were maintained at 20°C according to standard protocols [47] and are listed in Table S3. All experiments used sodium hypochlorite treatment (1.2% NaOCl, 250 mM KOH) to obtain synchronized L1 larvae [47]. L4 larvae were analyzed 40 to 48 hr after L1 stage. Day 1 and day 2 adults were analyzed 72 and 96 hr after L1 stage, respectively. Finer developmental staging was achieved by gonad morphology using the following criteria: early L4, distal gonad arm has turned and begun retrograde migration but was shorter than

half the length of the proximal arm; mid L4, distal and proximal gonad arms were approximately the same length; late L4, distal gonad arm was longer than the proximal and spermatogenesis was visible in the proximal gonad; and YA, enlarged oocytes were present in the proximal gonad, but no fertilized embryos were yet in the uterus. RNAi depletion was performed by feeding, as described previously [48]. In brief, synchronized L1 larvae were added to RNAi feeding plates, kept at 20°C, and analyzed 48 hr later for L4-stage larvae or 72 hr later for 1-day-old adults. CYC-1 depletion from the L1 stage severely delayed development and inhibited GSPC divisions. Consequently, synchronized L1 larvae were added to standard OP50 plates for 24 hr before being transferred to RNAi feeding plates and were analyzed 48 hr later. The following clones from the Arhinger library were used: sjj_C50F4.11 (*mdf-1/Mad1*), sjj_R12B2.4 (*him-10/Nuf2*), sjj_T10E9.7 (*nuo-2*), and sjj_C54G4.8 (*cyc-1*). The empty vector L4440 was used as a control. All clones were verified by sequencing.

### Dietary Restriction

Reported durations of congression are from L4-stage GSPCs, with the exception of *eat-2* mutant data in Figure 3E, which are from 1-day-old adults. sDR also delayed mitotic progression in adult GSPCs (data not shown). *eat-2(ad465)* animals were raised on control RNAi (L4440) feeding plates to allow for comparison with gene depletions. For sDR, a fresh OP50 overnight culture was diluted 1:10 in S basal medium, and 150 μl was added per standard 35 mm plate, containing 0.05 mg/ml carbenicillin to prevent additional OP50 growth. 150 μl of the undiluted culture was used as a control. Plates were dried for approximately 1 hr at room temperature, and 15–25 synchronized L1 larvae were added per plate. L4-stage animals were analyzed 48 hr after L1. For adult analyses, an additional 150 μl of bacteria was added after 2 days to prevent complete starvation.

### Worm Mounting and Live Imaging

Animals were anaesthetized in 0.04% tetramisole (Sigma) in M9 buffer and transferred to a 3% agarose pad, molded with 20- to 80-μm-wide grooves made by a custom nanofabricated silica plate, onto which a coverslip was placed. The chamber was backfilled with M9 buffer containing 0.04% tetramisole and sealed using VaLaP (1:1:1 Vaseline, lanolin, and paraffin). Imaging of GSPCs expressing the β-tub::GFP transgene alone was carried out on a Nikon A1R point scanning confocal microscope (Nikon Canada) using an Apo 40×/1.25 numerical aperture (NA) water-immersion objective. A z stack through the entire distal gonad (18–25 0.75-μm sections) was acquired every 30 s for 30 to 60 min using NIS-Elements software (Nikon). These imaging conditions did not appear to affect mitotic progression, as mitotic timing was largely independent of when, relative to the start of image acquisition, a division occurred (data not shown). Two-color time-lapse movies (β-tub::GFP, H2B::mCh and CYB-1::YFP, H2B::mCh) were acquired on a swept field confocal microscope (Nikon Canada and Prairie Technologies) using a Plan-Apo 60×/1.4 NA oil-immersion objective and a CoolSnap HQ2 CCD camera (Photometrics). z stacks of 9–13 0.75 μm sections were acquired in NIS Elements software (Nikon) every 30 s for 30 to 60 min using 2 × 2 binning, 400 ms exposure, and the 70 μm confocal slit aperture.

### Analysis of Mitotic Progression from Spindle Length

Pairs of β-tub::GFP-positive centrosomes were identified using the Spots segmentation tool in Imaris (Bitplane). The distance between paired centrosomes in three dimensions over time was extracted using custom MATLAB-based software. Analysis of spindle length was carried out in Excel. A least-squares line was plotted through all time points during which spindle length was at a constant minimum and three to four time points covering the decrease and increase in spindle length prior to and following this period. The duration of congression was calculated from the points of intersection of these three lines. For Table 1, we considered "prophase" as the time from the start of centrosome separation/migration to the start of congression, "anaphase" as the time between the end of congression and the end of spindle elongation, "spindle length" as the mean spindle length during congression, "maximum spindle length" as the average spindle length after the end of spindle elongation, and the "rate of spindle elongation" as the slope of a least-squares line through the first 1.5 min of spindle elongation (the rapid phase of spindle elongation), with spindle length normalized to metaphase length and plotted as a function of time after anaphase onset. To express the two phases of spindle elongation as a single variable (referred to as "pole separation"), we calculated spindle length (normalized to metaphase spindle length) 2.5 min after the start of spindle elongation from the least-squares line through this and two flanking time points. The mitotic index per gonad arm was approximated by counting the number of GSPCs at the start of each time lapse with two clearly defined centrosomes and dividing by the total number of GSPCs for each developmental stage as previously reported [17, 34].

### Analysis of Mitotic Progression from H2B::mCh Variance

Image processing and data extraction were carried out in ImageJ (NIH). Data analysis was performed in Excel. z stacks were background subtracted using a rolling ball kernel radius of 15 pixels, and average-intensity projections of the three to four optical slices containing the nucleus of interest were generated. Using a fixed 19-pixel diameter circular region of interest (ROI), we manually tracked individual nuclei and extracted the mean intensity and SD of the H2B::mCh signal at each time point. Prior to the start of visible chromosome condensation, the H2B::mCh signal was relatively uniform across the ROI and the variance (SD) was low. As chromosomes condensed and congressed, the H2B::mCh signal variance increased sharply as signal intensity became concentrated at the metaphase plate. Signal variance was normalized to its maximum, and we set the start and end of congression as the first and last time point, respectively, when variance exceeded 65% of maximum.

### Analysis of CYB-1::YFP Degradation Kinetics

Image processing and extraction of fluorescence intensities were carried out in ImageJ (NIH) as described above, using the H2B::mCh channel to define ROIs. Data analysis was performed using Excel and MATLAB. CYB-1::YFP intensity measurements were made in 74 non-dividing cells from 24 gonads, and these data were used to construct a standard photobleach correction curve, which was applied to all cells analyzed. Background signal was calculated on a per cell basis by averaging of all data points after the end of signal degradation. Photobleach-corrected and background-subtracted values were normalized to the value at the start of congression, and time was expressed relative to anaphase onset (both determined by H2B::mCh variance; see above). Normalized decay curves were fit using MATLAB and a Boltzmann sigmoid equation, $y = A2 + (A1 - A2) / (1 + \exp((x - T50) / dx))$, where A1 is the upper asymptote, A2 is the lower asymptote, T50 is the time to half maximum, and dx is the rate constant).

### Embryonic Lethality and Larval Lethality and/or Arrest Assay

Synchronized control (UM225) and *eat-2(ad465)* (UM272) L1 larvae were raised on L4440 or *Mad1* RNAi plates. Four days after L1, single adults were transferred to fresh plates, allowed to lay eggs for 8 hr, and then removed. Eggs were counted at the end of the 8 hr collection. Percent embryonic lethality was calculated as the number of unhatched eggs 24 hr after the end of the egg collection divided by the total number of eggs laid. Percent larval lethality and/or arrest was calculated as the total number of mature adults present 5 days after the egg collection divided by the total number of eggs laid. The progeny of 20 individual animals from two independent experiments were analyzed.

### *xol-1::GFP* Reporter Assay

Synchronized control (TY2441) and *Mad2* (UM364) L1 larvae were subjected to sDR for 4 days. Animals were then anaesthetized in M9 buffer containing 0.02% tetramisole (Sigma) and imaged on a Zeiss Axioimager Z1 microscope (Carl Zeiss Canada) with a Zeiss HRM camera and a Plan-Apo 20×/0.8 NA air objective. Images were analyzed in Image J (NIH) by counting of the number of embryos in utero per worm with fluorescence levels above a universally applied threshold pixel intensity. At least 100 worms were analyzed per condition.

### Graphing and Statistical Analysis

Graphing and statistical analysis were performed in MATLAB. Pair-wise comparisons were analyzed using a two-tailed Student's t test, with the exception of *xol-1::GFP* data (Figure 3F), for which a two-sided Wilcoxon rank-sum test was used. Where multiple means were compared, ANOVA1 with a Tukey-Kramer post hoc test was applied. Correlations are reported as Pearson's linear correlation coefficient (r), and statistical significance was determined

using Student's t distribution. For all figures, *p < 0.05, **p < 0.01, and ***p < 0.001; n.s., p > 0.05.

## SUPPLEMENTAL INFORMATION

Supplemental Information includes Supplemental Experimental Procedures, four figures, three tables, and three movies and can be found with this article online at http://dx.doi.org/10.1016/j.cub.2015.02.054.

## AUTHOR CONTRIBUTIONS

A.R.G. designed, carried out, and analyzed all experiments with input from J.-C.L. and P.S.M., with the exception of NUO-2 and CYC-1 depletion (J.-N.V.-T.) and with assistance from J.R. for the CYB-1::YFP assay. J.F.D. wrote the custom MATLAB script to derive spindle lengths from segmented Imaris movies. A.R.G. wrote the manuscript with input from all authors. J.-C.L. and P.S.M. devised the initial project to use live imaging to study germ cell mitosis in situ.

## ACKNOWLEDGMENTS

We thank A. Desai, A. Golden, M. Zetka, and the *Caenorhabditis* Genetics Center for strains, J. Khanikar and D. P. Salazar Ospina for conducting early experiments to assess the feasibility of live-imaging germ cell mitosis and C. Charbonneau of IRIC's Bio-imaging facility for technical assistance. We are grateful to A.S. Maddox, E.D. Salmon, and M. Peifer for comments on the manuscript and to members of the J.-C.L. and P.S.M. labs for helpful discussions. This work was funded by a grant from the CIHR (MOP-115171) to J.-C.L. and P.S.M. J.-C.L. holds the Canada Research Chair in Cell Division and Differentiation. P.S.M. is supported as a William Burwell Harrison Fellow of Biology. IRIC is supported in part by the Canada Foundation for Innovation and the Fonds de Recherche du Québec-Santé.

Received: December 22, 2014
Revised: February 15, 2015
Accepted: February 19, 2015
Published: March 26, 2015

## REFERENCES

1. Rashidi, N.M., Scott, M.K., Scherf, N., Krinner, A., Kalchschmidt, J.S., Gounaris, K., Selkirk, M.E., Roeder, I., and Lo Celso, C. (2014). In vivo time-lapse imaging shows diverse niche engagement by quiescent and naturally activated hematopoietic stem cells. Blood *124*, 79–83.
2. Ritsma, L., Ellenbroek, S.I., Zomer, A., Snippert, H.J., de Sauvage, F.J., Simons, B.D., Clevers, H., and van Rheenen, J. (2014). Intestinal crypt homeostasis revealed at single-stem-cell level by in vivo live imaging. Nature *507*, 362–365.
3. Rompolas, P., Mesa, K.R., and Greco, V. (2013). Spatial organization within a niche as a determinant of stem-cell fate. Nature *502*, 513–518.
4. Roostalu, J., Schiebel, E., and Khmelinskii, A. (2010). Cell cycle control of spindle elongation. Cell Cycle *9*, 1084–1090.
5. Cinquin, O., Crittenden, S.L., Morgan, D.E., and Kimble, J. (2010). Progression from a stem cell-like state to early differentiation in the C. elegans germ line. Proc. Natl. Acad. Sci. USA *107*, 2048–2053.
6. Kimble, J. (2011). Molecular regulation of the mitosis/meiosis decision in multicellular organisms. Cold Spring Harb. Perspect. Biol. *3*, a002683.
7. Crittenden, S.L., Leonhard, K.A., Byrd, D.T., and Kimble, J. (2006). Cellular analyses of the mitotic region in the *Caenorhabditis elegans* adult germ line. Mol. Biol. Cell *17*, 3051–3061.
8. Fox, P.M., Vought, V.E., Hanazawa, M., Lee, M.H., Maine, E.M., and Schedl, T. (2011). Cyclin E and CDK-2 regulate proliferative cell fate and cell cycle progression in the *C. elegans* germline. Development *138*, 2223–2234.
9. Hubbard, E.J. (2007). *Caenorhabditis elegans* germ line: a model for stem cell biology. Dev. Dyn. *236*, 3343–3357.
10. Kimble, J., and Crittenden, S.L. (2007). Controls of germline stem cells, entry into meiosis, and the sperm/oocyte decision in *Caenorhabditis elegans*. Annu. Rev. Cell Dev. Biol. *23*, 405–433.
11. Kimble, J.E., and White, J.G. (1981). On the control of germ cell development in *Caenorhabditis elegans*. Dev. Biol. *81*, 208–219.
12. Encalada, S.E., Willis, J., Lyczak, R., and Bowerman, B. (2005). A spindle checkpoint functions during mitosis in the early *Caenorhabditis elegans* embryo. Mol. Biol. Cell *16*, 1056–1070.
13. Essex, A., Dammermann, A., Lewellyn, L., Oegema, K., and Desai, A. (2009). Systematic analysis in *Caenorhabditis elegans* reveals that the spindle checkpoint is composed of two largely independent branches. Mol. Biol. Cell *20*, 1252–1267.
14. Kitagawa, R. (2009). The spindle assembly checkpoint in *Caenorhabditis elegans*: one who lacks Mad1 becomes mad one. Cell Cycle *8*, 338–344.
15. Ables, E.T., Laws, K.M., and Drummond-Barbosa, D. (2012). Control of adult stem cells *in vivo* by a dynamic physiological environment: diet-dependent systemic factors in *Drosophila* and beyond. Wiley Interdiscip. Rev. Dev. Biol. *1*, 657–674.
16. Hubbard, E.J., Korta, D.Z., and Dalfó, D. (2013). Physiological control of germline development. Adv. Exp. Med. Biol. *757*, 101–131.
17. Killian, D.J., and Hubbard, E.J. (2005). *Caenorhabditis elegans* germline patterning requires coordinated development of the somatic gonadal sheath and the germ line. Dev. Biol. *279*, 322–335.
18. Oegema, K., Desai, A., Rybina, S., Kirkham, M., and Hyman, A.A. (2001). Functional analysis of kinetochore assembly in *Caenorhabditis elegans*. J. Cell Biol. *153*, 1209–1226.
19. Desai, A., Rybina, S., Müller-Reichert, T., Shevchenko, A., Shevchenko, A., Hyman, A., and Oegema, K. (2003). KNL-1 directs assembly of the microtubule-binding interface of the kinetochore in *C. elegans*. Genes Dev. *17*, 2421–2435.
20. Deyter, G.M., Furuta, T., Kurasawa, Y., and Schumacher, J.M. (2010). *Caenorhabditis elegans* cyclin B3 is required for multiple mitotic processes including alleviation of a spindle checkpoint-dependent block in anaphase chromosome segregation. PLoS Genet. *6*, e1001218.
21. Espeut, J., Cheerambathur, D.K., Krenning, L., Oegema, K., and Desai, A. (2012). Microtubule binding by KNL-1 contributes to spindle checkpoint silencing at the kinetochore. J. Cell Biol. *196*, 469–482.
22. Yamamoto, T.G., Watanabe, S., Essex, A., and Kitagawa, R. (2008). SPDL-1 functions as a kinetochore receptor for MDF-1 in *Caenorhabditis elegans*. J. Cell Biol. *183*, 187–194.
23. Musacchio, A., and Salmon, E.D. (2007). The spindle-assembly checkpoint in space and time. Nat. Rev. Mol. Cell Biol. *8*, 379–393.
24. Meraldi, P., Draviam, V.M., and Sorger, P.K. (2004). Timing and checkpoints in the regulation of mitotic progression. Dev. Cell *7*, 45–60.
25. Rodriguez-Bravo, V., Maciejowski, J., Corona, J., Buch, H.K., Collin, P., Kanemaki, M.T., Shah, J.V., and Jallepalli, P.V. (2014). Nuclear pores protect genome integrity by assembling a premitotic and Mad1-dependent anaphase inhibitor. Cell *156*, 1017–1031.
26. DeLuca, J.G., Moree, B., Hickey, J.M., Kilmartin, J.V., and Salmon, E.D. (2002). hNuf2 inhibition blocks stable kinetochore-microtubule attachment and induces mitotic cell death in HeLa cells. J. Cell Biol. *159*, 549–555.
27. Howe, M., McDonald, K.L., Albertson, D.G., and Meyer, B.J. (2001). HIM-10 is required for kinetochore structure and function on Caenorhabditis elegans holocentric chromosomes. J. Cell Biol. *153*, 1227–1238.
28. Kitagawa, R., and Rose, A.M. (1999). Components of the spindle-assembly checkpoint are essential in *Caenorhabditis elegans*. Nat. Cell Biol. *1*, 514–521.
29. Stevens, D., Oegema, K., and Desai, A. (2013). Meiotic double-strand breaks uncover and protect against mitotic errors in the *C. elegans* germline. Curr. Biol. *23*, 2400–2406.
30. Collin, P., Nashchekina, O., Walker, R., and Pines, J. (2013). The spindle assembly checkpoint works like a rheostat rather than a toggle switch. Nat. Cell Biol. *15*, 1378–1385.

  

31. Dick, A.E., and Gerlich, D.W. (2013). Kinetic framework of spindle assembly checkpoint signalling. Nat. Cell Biol. *15*, 1370–1377.

32. Clute, P., and Pines, J. (1999). Temporal and spatial control of cyclin B1 destruction in metaphase. Nat. Cell Biol. *1*, 82–87.

33. Greer, E.L., Dowlatshahi, D., Banko, M.R., Villen, J., Hoang, K., Blanchard, D., Gygi, S.P., and Brunet, A. (2007). An AMPK-FOXO pathway mediates longevity induced by a novel method of dietary restriction in *C. elegans*. Curr. Biol. *17*, 1646–1656.

34. Korta, D.Z., Tuck, S., and Hubbard, E.J. (2012). S6K links cell fate, cell cycle and nutrient response in C. elegans germline stem/progenitor cells. Development *139*, 859–870.

35. Houthoofd, K., Braeckman, B.P., Lenaerts, I., Brys, K., Matthijssens, F., De Vreese, A., Van Eygen, S., and Vanfleteren, J.R. (2005). DAF-2 pathway mutations and food restriction in aging *Caenorhabditis elegans* differentially affect metabolism. Neurobiol. Aging *26*, 689–696.

36. Cross, R.A., and McAinsh, A. (2014). Prime movers: the mechanochemistry of mitotic kinesins. Nat. Rev. Mol. Cell Biol. *15*, 257–271.

37. Maiato, H., and Lince-Faria, M. (2010). The perpetual movements of anaphase. Cell. Mol. Life Sci. *67*, 2251–2269.

38. Dillin, A., Hsu, A.L., Arantes-Oliveira, N., Lehrer-Graiwer, J., Hsin, H., Fraser, A.G., Kamath, R.S., Ahringer, J., and Kenyon, C. (2002). Rates of behavior and aging specified by mitochondrial function during development. Science *298*, 2398–2401.

39. Kelly, K.O., Dernburg, A.F., Stanfield, G.M., and Villeneuve, A.M. (2000). *Caenorhabditis elegans msh-5* is required for both normal and radiation-induced meiotic crossing over but not for completion of meiosis. Genetics *156*, 617–630.

40. Nicoll, M., Akerib, C.C., and Meyer, B.J. (1997). X-chromosome-counting mechanisms that determine nematode sex. Nature *388*, 200–204.

41. Houthoofd, K., Braeckman, B.P., Lenaerts, I., Brys, K., De Vreese, A., Van Eygen, S., and Vanfleteren, J.R. (2002). Ageing is reversed, and metabolism is reset to young levels in recovering dauer larvae of C. elegans. Exp. Gerontol. *37*, 1015–1021.

42. Pines, J. (2006). Mitosis: a matter of getting rid of the right protein at the right time. Trends Cell Biol. *16*, 55–63.

43. Rieder, C.L., and Maiato, H. (2004). Stuck in division or passing through: what happens when cells cannot satisfy the spindle assembly checkpoint. Dev. Cell *7*, 637–651.

44. Masoro, E.J. (2005). Overview of caloric restriction and ageing. Mech. Ageing Dev. *126*, 913–922.

45. Hanahan, D., and Weinberg, R.A. (2011). Hallmarks of cancer: the next generation. Cell *144*, 646–674.

46. López-Otín, C., Blasco, M.A., Partridge, L., Serrano, M., and Kroemer, G. (2013). The hallmarks of aging. Cell *153*, 1194–1217.

47. Brenner, S. (1974). The genetics of *Caenorhabditis elegans*. Genetics *77*, 71–94.

48. Kamath, R.S., Martinez-Campos, M., Zipperlen, P., Fraser, A.G., and Ahringer, J. (2001). Effectiveness of specific RNA-mediated interference through ingested double-stranded RNA in Caenorhabditis elegans. Genome Biol. *2*, RESEARCH0002.


 